

An Adaptive Stable Space-Time FE Method for the Shallow Water Equations

Eirik Valseeth*, Clint Dawson

Oden Institute for Computational Engineering and Sciences, The University of Texas at Austin, Austin, TX 78712, USA

Abstract

We consider the finite element (FE) approximation of the shallow water equations (SWE) by considering discretizations in which both space and time are established using an unconditionally stable FE method. Particularly, we consider the automatic variationally stable FE (AVS-FE) method, a type of discontinuous Petrov-Galerkin (DPG) method. The philosophy of the DPG method allows us to break the test space and achieve unconditionally stable FE approximations as well as accurate *a posteriori* error estimators upon solution of a saddle point system of equations. The resulting error indicators allow us to employ mesh adaptive strategies and perform space-time mesh refinements, i.e., local time stepping.

We derive *a priori* error estimates for the AVS-FE method and linearized SWE and perform numerical verifications to confirm corresponding asymptotic convergence behavior. In an effort to keep the computational cost low, we consider an alternative space-time approach in which the space-time domain is partitioned into finite sized space-time slices. Hence, we can perform adaptivity on each individual slice to preset error tolerances as needed for a particular application. Numerical verifications comparing the two alternatives indicate the space-time slices are superior for simulations over long times, whereas the solutions are indistinguishable for short times. Multiple numerical verifications show the adaptive mesh refinement capabilities of the AVS-FE method, as well the application of the method to commonly applied benchmarks for the SWE.

Keywords: Shallow water equations, discontinuous Petrov-Galerkin, Adaptivity, Space-Time FE method, Local time stepping

2000 MSC: 65M60 35A35 35L65 35Q35

1. Introduction

The shallow water equations govern the flow of water in domains in which the characteristic wavelength horizontally is significantly larger than the depth of water. A very important application of the SWE is in the modeling of events such as storm surges resulting from hurricanes. Thus, the importance of accurate numerical solution techniques should therefore be clear as the repercussions of such events can be vast. The SWE are models for the Navier-Stokes equations in which the direction of the depth has been integrated from the sea floor to the free surface of the water and

*Corresponding author

Email addresses: Eirik@utexas.edu (Eirik Valseeth), Clint@oden.utexas.edu (Clint Dawson)

application of the corresponding boundary conditions. The resulting equations are continuity and momentum equations for the water surface elevation and depth-averaged horizontal velocities, respectively. Generally, the domains of interest in the application of the SWE are irregular and the resulting computational meshes need to be unstructured, thereby making FE methods well suited for the numerical approximation of the SWE, see, e.g., [1, 2] for early examples.

For flow regimes resulting from hurricanes, the motion of the water, i.e., convection is the driving mechanism of transport. The domination of convective transport over diffusive transport leads to stability issues in classical Galerkin FE methods. This issue is well known to be resolved when the element size in the FE mesh is adequately refined near the interior or boundary layers induced by this phenomenon. However, the computational cost and the required mesh generation efforts on a case-by-case basis is generally prohibitive. Furthermore, the smallest element size dictates the corresponding time step size further increasing the computational cost. Lynch and Gray developed the wave continuity equation as a surrogate for the SWE in [3] which result in more stable FE approximations as it changes the enforcement of the continuity equation by introducing second order time derivatives thereby circumventing the hyperbolic nature of the SWE. The wave continuity equation is employed in the advanced circulation model of Luettich *et. al* [4], which is widely used and has been developed to encompass a wide range of features important in hurricane storm surge modeling.

Discontinuous Galerkin (DG) methods as well as their hybridized versions [5–7] are popular FE methods for the SWE. Important reasons for their popularity include high accuracy, their mass conservation property, ease of establishing conditionally stable FE discretizations, and local p -adaptivity [8]. Recently, high order entropy stable DG methods for curved FE meshes have been introduced for the SWE by Wu *et al.* in [9] which satisfies discrete conservation of entropy. The entropy stable method takes advantage of summation-by-parts operators to increase computational efficiency compared to traditional DG methods demonstrated through numerical verifications. The development of hybridized DG (HDG) methods has also reduced the computational cost of solving the global system of equations compared to classical DG methods [5]. Coupled Galerkin and DG methods have also successfully been developed to maximize efficiency and accuracy by Dawson and Proft in [10, 11]. Least squares FE methods (LSFEMs) [12] have also been successfully applied to the SWE by Starke in [13] and Liang and Hsu in [14]. Both these LSFEMs take advantage of the stability property of LSFEMs spatially and the authors present several numerical verifications.

All the aforementioned FE methods used in shallow water systems for the SWE or its surrogate wave continuity equation employ a method of lines approach in the temporal discretization. Thus, spatial and temporal computations are decoupled, where finite elements are employed in space and time stepping schemes such as finite difference methods are employed in time. It is significantly less common to employ space-time FE methods, i.e., using FE discretizations of both space and time. The main reasons are likely the increased computational cost of such methods, as well as the inherently unstable numerical nature of classical FE methods for first order partial derivatives. However, some examples of space-time FE methods for the SWE do exist in literature [15–18], where conditional discrete stability is ensured in space and time by an upwinding argument. In modern multi processor computers and supercomputers, the additional cost of space-time FE methods can be justified as the functional framework of FE leads to

readily available *a priori* error bounds in addition to *a posteriori* error estimation techniques. Hence, space-time FE methods can take advantage of adaptive mesh refinement strategies to ensure maximum computational efficiency and accuracy.

The AVS-FE method [19] is an unconditionally stable FE method that falls into the category of discontinuous Petrov-Galerkin (DPG) methods, introduced by Demkowicz and Gopalakrishnan [20–24]. The unconditional stability of the method is ensured by a particular choice of test functions which is defined by a Riesz representation problem that realize the supremum in the *inf-sup* condition. Hence, the AVS-FE method is a Petrov-Galerkin method in which the weak formulation is such that the trial space is a globally continuous Hilbert space, whereas the test space is a broken Hilbert space. Hence, the test functions are square integrable functions that are of higher order regularity on each element, e.g., H^1 or $H(\text{div})$. The corresponding FE discretization of this test space is achieved by computing on-the-fly optimal test functions in the spirit of the DPG method. This method remains attractive in particular due to its unconditional stability property, regardless of the differential operator. Additionally, according to the philosophy of the DPG method, the AVS-FE method establishes an equivalent saddle point system which yields both the AVS-FE approximation, as well as an "error representation function". This function leads to *a posteriori* error estimates of the numerical approximation error in terms of the energy norm induced by the sesquilinear form.

In this paper, we build upon the work of [25], where the AVS-FE method was employed to establish space-time FE approximations for the Korteweg-de Vries equation. Following this introduction, we introduce the model initial boundary value problem (IBVP) as well as notations and conventions in Section 2.1. In Section 2.2, we present the equivalent AVS-FE weak formulation and its analysis for the SWE IBVP as well as the concepts of Carstensen *et al.* [26] to establish nonlinear AVS-FE approximations. *A priori* error estimates are introduced in Section 3. In Section 4, we perform multiple numerical verifications for the SWE presenting numerical asymptotic convergence properties as well h -adaptive mesh refinements. Finally, we conclude with remarks on the results and future works in Section 5.

2. The Shallow Water Equations and the AVS-FE Method

We consider a simplified form of the SWE to establish an unconditionally stable space-time FE method for the SWE. After establishing the SWE model problem, we introduce the corresponding AVS-FE weak formulation and discretization.

2.1. Model Problem: The Shallow Water Equations

The derivation of the SWE from the three-dimensional incompressible Navier–Stokes equations is performed under the assumptions of a long horizontal wavelength and a hydrostatic pressure distribution, see, e.g. [27]. Let $\Omega \subset \mathbb{R}^2$ be a bounded open domain with a Lipschitz boundary $\partial\Omega$ which is partitioned into two segments Γ_I and Γ_O , such that $\partial\Omega = \overline{\Gamma_I \cup \Gamma_O}$. Also, let \mathbf{n} be the outwards unit normal vector to the global boundary, and identify the boundary segments as $\Gamma_I = \{\mathbf{x} \in \partial\Omega : \mathbf{u} \cdot \mathbf{n} < 0\}$ and $\Gamma_O = \{\mathbf{x} \in \partial\Omega : \mathbf{u} \cdot \mathbf{n} \geq 0\}$ as in and outflow boundaries, respectively.

Finally, define the temporal domain $t \in (0, T) \subset \mathbb{R}_0^+$. Hence, we consider the following version of the viscous two dimensional SWE [10, 11]:

$$\frac{\partial \zeta}{\partial t} + \nabla \cdot (\mathbf{H}\mathbf{u}) = 0, \quad (1a)$$

$$\frac{\partial \mathbf{u}}{\partial t} + \mathbf{u} \cdot (\nabla \mathbf{u}) + \tau_{bf} \mathbf{u} + g \nabla \zeta - \mu \Delta \mathbf{u} = \mathbf{f}, \quad (1b)$$

where $H = \zeta + h_b$, $h_b = h_b(\mathbf{x})$ is the bathymetry of the bottom surface (see Figure 1), the unknowns $\zeta = \zeta(\mathbf{x}, t)$ and $\mathbf{u} = \mathbf{u}(\mathbf{x}, t) = \{u_x(\mathbf{x}, t), u_y(\mathbf{x}, t)\}^T$ represent depth averaged elevation and velocity, respectively, $g = 9.81m/s^2$ the constant of gravitational acceleration, μ the depth averaged turbulent viscosity, τ_{bf} the bottom friction factor, and \mathbf{f} represent body forces. The system (1) consists of two partial differential equations (PDEs), the continuity

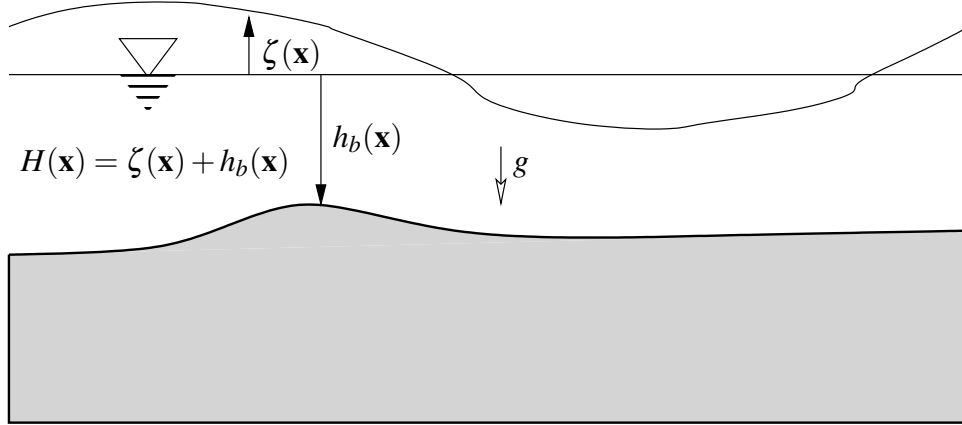


Figure 1: Elevation and bathymetry overview.

equation (1a) for the depth averaged water column elevation, and the momentum equation (1b) governing the depth averaged velocity. The bottom friction factor τ_b is a source of another potential nonlinearity as multiple friction models depend on both velocity and water depth.

To establish an IBVP of the SWE with a unique solution, a proper combination of boundary conditions (BCs) and initial conditions (ICs) is needed. Since the SWE are derived from the Navier-Stokes equations, these conditions are often not trivial to establish due to the chaotic nature of these PDEs. In this paper, we seek to establish stable FE approximations of the SWE, therefore, for simplicity, we only consider cases in which the resulting IBVP has a unique solution [28]. To this end, we consider the following boundary and initial conditions:

$$\begin{aligned} \zeta &= \hat{\zeta} \text{ on } \Gamma_I, \\ \mathbf{u} &= \hat{\mathbf{u}} \text{ on } \partial\Omega, \\ \zeta &= \zeta_0 \text{ on } \Omega, \\ \mathbf{u} &= \mathbf{u}_0 \text{ on } \Omega. \end{aligned} \quad (2)$$

Combining the PDE (1) and the conditions (2) gives the SWE IBVP:

Find (ζ, \mathbf{u}) such that:

$$\begin{aligned} \frac{\partial \zeta}{\partial t} + \nabla \cdot (\mathbf{H}\mathbf{u}) &= 0, \text{ in } \Omega \times (0, T), \\ \frac{\partial \mathbf{u}}{\partial t} + \mathbf{u} \cdot (\nabla \mathbf{u}) + \tau_{bf} \mathbf{u} + g \nabla \zeta - \mu \Delta \mathbf{u} &= \mathbf{f}, \text{ in } \Omega \times (0, T), \end{aligned}$$

$$\begin{aligned} \zeta &= \hat{\zeta} \text{ on } \Gamma_I, \\ \mathbf{u} &= \hat{\mathbf{u}} \text{ on } \partial\Omega, \\ \zeta &= \zeta_0 \text{ on } \Omega, \\ \mathbf{u} &= \mathbf{u}_0 \text{ on } \Omega. \end{aligned}$$

(3)

In the following, we shall use the following notations:

- inner products between vector valued functions are denoted with the single dot symbol “.”, and inner products between tensor valued functions are denoted by the colon or double dot symbol “:”.
- the operator ∇ is the spatial gradient operator.
- the operation $\nabla \cdot \boldsymbol{\sigma}$, $\boldsymbol{\sigma}$ being a matrix/tensor valued function, corresponds to a row-wise application of the gradient operator.
- h_m is the diameter of element K_m .
- \mathbf{n}_m is the outwards unit normal vector to element K_m .

2.2. Weak Formulation and AVS-FE Discretization

The derivation of a weak formulation for the AVS-FE method can be found in [19] and we omit the step-by-step derivation found in these for the SWE and mention key points only. The AVS-FE weak formulations are established by techniques used in mixed FE methods as well as the broken weak forms associated to DPG and DG methods. The first step is the partition of the computational domain into finite elements, i.e., into a FE mesh. Since we are taking a space-time approach, we first define the space-time domain Ω_T :

$$\Omega_T \stackrel{\text{def}}{=} \Omega \times (0, T),$$

and the partition \mathcal{P}_h of Ω_T into elements K_m , is such that:

$$\Omega_T = \text{int} \left(\bigcup_{K_m \in \mathcal{P}_h} \overline{K_m} \right), \quad K_m \cap K_n, \quad m \neq n. \quad (4)$$

Our goal is to employ classical continuous FE approximating functions as bases for the trial space, e.g., Lagrange or Raviart-Thomas functions. Hence, it is required to recast the IBVP (3) into a first order system by introducing a tensor-valued auxiliary variable $\boldsymbol{\sigma}$:

$$\boldsymbol{\sigma} = \nabla \mathbf{u} \stackrel{\text{def}}{=} \begin{bmatrix} \frac{\partial u_x}{\partial x} & \frac{\partial u_x}{\partial y} \\ \frac{\partial u_y}{\partial x} & \frac{\partial u_y}{\partial y} \end{bmatrix}. \quad (5)$$

Using this variable, we recast the SWE IBVP as:

Find $(\zeta, \mathbf{u}, \boldsymbol{\sigma})$ such that:

$$\begin{aligned} \frac{\partial \zeta}{\partial t} + \nabla \cdot (\mathbf{H}\mathbf{u}) &= 0, \text{ in } \Omega_T, \\ \frac{\partial \mathbf{u}}{\partial t} + \mathbf{u} \cdot (\nabla \mathbf{u}) + \tau_{bf} \mathbf{u} + g \nabla \zeta - \mu \nabla \cdot \boldsymbol{\sigma} &= \mathbf{f}, \text{ in } \Omega_T, \\ \boldsymbol{\sigma} - \nabla \mathbf{u} &= \mathbf{0}, \text{ in } \Omega_T, \end{aligned} \tag{6}$$

$$\begin{aligned} \zeta &= \hat{\zeta} \text{ on } \Gamma_1, \\ \mathbf{u} &= \hat{\mathbf{u}} \text{ on } \partial\Omega, \\ \zeta &= \zeta_0 \text{ on } \Omega_0, \\ \mathbf{u} &= \mathbf{u}_0 \text{ on } \Omega_0. \end{aligned}$$

Hence, in the weak enforcement of (6), the required regularities of the trial variables are $\zeta \in H^1(\Omega_T)$, $\mathbf{u} \in H^1(\Omega_T)^2$, and $\boldsymbol{\sigma} \in H(\mathbf{div}, \Omega)$, where $H^1(\Omega_T)$ and $H(\mathbf{div}, \Omega)$ are the classical H^1 and $H(\mathbf{div})$ Hilbert spaces on Ω_T and Ω , respectively.

The AVS-FE weak formulation is established by an element-wise weak enforcement of (6), application of Green's identity to all spatial derivatives with the exception of the convective term $\mathbf{u} \cdot (\nabla \mathbf{u})$. The BCs are all enforced in a weak sense, and we incorporate the initial conditions strongly in the definitions of the trial space. Thus, the AVS-FE weak formulation is:

Find $(\zeta, \mathbf{u}, \boldsymbol{\sigma}) \in U(\Omega_T)$ such that:

$$B((\zeta, \mathbf{u}, \boldsymbol{\sigma}); (v, \mathbf{w}, \mathbf{p})) = F(v, \mathbf{w}, \mathbf{p}), \quad \forall (v, \mathbf{w}, \mathbf{p}) \in V(\mathcal{P}_h), \tag{7}$$

where the sesquilinear form, $B : U(\Omega_T) \times V(\mathcal{P}_h) \rightarrow \mathbb{R}$, and linear functional, $F : V(\mathcal{P}_h) \rightarrow \mathbb{R}$ are defined:

$$\begin{aligned} B((\zeta, \mathbf{u}, \boldsymbol{\sigma}), (v, \mathbf{w}, \mathbf{p})) &\stackrel{\text{def}}{=} \sum_{K_m \in \mathcal{P}_h} \int_{K_m} \left\{ \frac{\partial \zeta}{\partial t} v_m - \nabla v_m \cdot (\mathbf{H}\mathbf{u}) \right. \\ &+ \left[\frac{\partial \mathbf{u}}{\partial t} + \mathbf{u} \cdot (\nabla \mathbf{u}) + \tau \mathbf{u} \right] \cdot \mathbf{w}_m - g \zeta (\nabla \cdot \mathbf{w}_m) + \mu \boldsymbol{\sigma} : \nabla \mathbf{w}_m \\ &+ \boldsymbol{\sigma} : \mathbf{p}_m + \mathbf{u} \cdot (\nabla \cdot \mathbf{p}_m) \left. \right\} \mathbf{d}\mathbf{x} + \oint_{\partial K_m} \left\{ v_m (\mathbf{H}\mathbf{u} \cdot \mathbf{n}_m) - \mu (\boldsymbol{\sigma} \mathbf{n}_m) \cdot \mathbf{w}_m \right\} \mathbf{d}s \\ &+ \oint_{\partial K_m \setminus \Gamma_{out}} g \zeta (\mathbf{w}_m \cdot \mathbf{n}_m) \mathbf{d}s, \\ F(v, \mathbf{w}, \mathbf{p}) &= \sum_{K_m \in \mathcal{P}_h} \int_{K_m} \mathbf{f} \cdot \mathbf{v}_m \mathbf{d}\mathbf{x} + \oint_{\partial K_m \cap \partial\Omega} (\hat{\mathbf{u}} \mathbf{p}_m) \cdot \mathbf{n}_m \mathbf{d}s - \oint_{\partial K_m \cap \Gamma_{in}} g \hat{\zeta} (\mathbf{w}_m \cdot \mathbf{n}_m) \mathbf{d}s, \end{aligned} \tag{8}$$

and the function spaces $U(\Omega_T)$ and $V(\mathcal{P}_h)$ are defined:

$$\begin{aligned} U(\Omega_T) &\stackrel{\text{def}}{=} \left\{ (\zeta, \mathbf{u}, \boldsymbol{\sigma}) \in H^1(\Omega_T)^3 \times H(\mathbf{div}, \Omega) : \mathbf{u}|_{\Omega_0} = \mathbf{u}_0, \zeta|_{\Omega_0} = \zeta_0 \right\}, \\ V(\mathcal{P}_h) &\stackrel{\text{def}}{=} H^1(\mathcal{P}_h)^3 \times H(\mathbf{div}, \mathcal{P}_h), \end{aligned} \tag{9}$$

where broken spaces are defined:

$$H^1(\mathcal{P}_h) \stackrel{\text{def}}{=} \left\{ v \in L^2(\Omega_T) : v_m \in H^1(K_m), \forall K_m \in \mathcal{P}_h \right\}, \tag{10}$$

$$H(\mathbf{div}, \mathcal{P}_h) \stackrel{\text{def}}{=} \left\{ \mathbf{v} \in L^2(\Omega)^4 : \mathbf{v}_m \in H(\mathbf{div}, K_m), \forall K_m \in \mathcal{P}_h \right\}. \quad (11)$$

We also define norms on these spaces, $\|\cdot\|_{U(\Omega)} : U(\Omega) \rightarrow [0, \infty)$ and $\|\cdot\|_{V(\mathcal{P}_h)} : V(\mathcal{P}_h) \rightarrow [0, \infty)$ as:

$$\|(\zeta, \mathbf{u}, \boldsymbol{\sigma})\|_{U(\Omega_T)} \stackrel{\text{def}}{=} \sqrt{\int_{\Omega} \left[\nabla \zeta \cdot \nabla \zeta + \zeta^2 + \nabla \mathbf{u} : \nabla \mathbf{u} + \mathbf{u} \cdot \mathbf{u} + (\nabla \cdot \boldsymbol{\sigma})^2 + \boldsymbol{\sigma} : \boldsymbol{\sigma} \right] \mathbf{d}\mathbf{x}}, \quad (12)$$

$$\|(v, \mathbf{w}, \mathbf{p})\|_{V(\mathcal{P}_h)} \stackrel{\text{def}}{=} \sqrt{\sum_{K_m \in \mathcal{P}_h} \int_{K_m} \left[h_m^2 \nabla v_m \cdot \nabla v_m + v_m \cdot v_m + h_m^2 \nabla \mathbf{w}_m : \nabla \mathbf{w}_m + \mathbf{w}_m \cdot \mathbf{w}_m + h_m^2 (\nabla \cdot \mathbf{p}_m)^2 + \mathbf{p}_m : \mathbf{p}_m \right] \mathbf{d}\mathbf{x}}.$$

Note that the norm $\|\cdot\|_{V(\mathcal{P}_h)}$ is equivalent to the classical broken norm:

$$\|(v, \mathbf{w}, \mathbf{p})\|_V \stackrel{\text{def}}{=} \sqrt{\sum_{K_m \in \mathcal{P}_h} \int_{K_m} \left[\nabla v_m \cdot \nabla v_m + v_m \cdot v_m + \nabla \mathbf{w}_m : \nabla \mathbf{w}_m + \mathbf{w}_m \cdot \mathbf{w}_m + (\nabla \cdot \mathbf{p}_m)^2 + \mathbf{p}_m : \mathbf{p}_m \right] \mathbf{d}\mathbf{x}}. \quad (13)$$

The weak formulation (7) is closely related to the weak formulations of the DPG method with ultraweak forms, differing in our choice of trial space.

To simplify the analyses of the AVS-FE weak formulation, we introduce an equivalent norm on the trial space, the energy norm $\|\cdot\|_B : U(\Omega_T) \rightarrow [0, \infty)$:

$$\|(\zeta, \mathbf{u}, \boldsymbol{\sigma})\|_B \stackrel{\text{def}}{=} \sup_{(v, \mathbf{w}, \mathbf{p}) \in V(\mathcal{P}_h) \setminus \{0\}} \frac{|B((\zeta, \mathbf{u}, \boldsymbol{\sigma}); (v, \mathbf{w}, \mathbf{p}))|}{\|(v, \mathbf{w}, \mathbf{p})\|_{V(\mathcal{P}_h)}}. \quad (14)$$

Before proceeding to the FE discretization of the weak formulation (7), we point out that the weak formulation is well posed as it satisfies the *inf-sup* and continuity conditions in terms of the energy norm with an *inf-sup* constant of unity if we consider a linearized version of the SWE for simplicity. Thus, the linearized form of this formulation satisfies the required conditions of the Babuška Lax-Milgram Theorem [29], for an in-depth discussion on broken spaces and variational forms we refer to [30]. We also define the optimal test functions $(\hat{e}, \hat{\boldsymbol{\varepsilon}}, \hat{\mathbf{E}}) \in V(\mathcal{P}_h)$, for each $(\zeta, \mathbf{u}, \boldsymbol{\sigma}) \in U(\Omega_T)$ as the solution of the Riesz representation problem:

$$((\hat{e}, \hat{\boldsymbol{\varepsilon}}, \hat{\mathbf{E}}); (v, \mathbf{w}))_{V(\mathcal{P}_h)} = B((\zeta, \mathbf{u}, \boldsymbol{\sigma}), (v, \mathbf{w}, \mathbf{p})), \quad \forall (v, \mathbf{w}, \mathbf{p}) \in V(\mathcal{P}_h). \quad (15)$$

The Riesz representation problem is well posed with unique solutions due to the inner product in the left hand side (LHS). Since (15) is infinite dimensional, the optimal test functions must be computed approximately through an FE approximation. Fortunately, since the test space is broken, the solution can be performed element wise, thereby removing the need for a global solve for the optimal test functions. While the definition of the energy norm makes the analysis of AVS-FE weak formulations straightforward, it is not computable as it is defined through a supremum. Thankfully, the definition of the optimal test functions through the Riesz representation problem ensures the following norm equivalence:

$$\|(\zeta, \mathbf{u}, \boldsymbol{\sigma})\|_B = \|(\hat{e}, \hat{\boldsymbol{\varepsilon}}, \hat{\mathbf{E}})\|_{V(\mathcal{P}_h)}, \quad (16)$$

which is readily available for computations once $(\hat{e}, \hat{\boldsymbol{\varepsilon}}, \hat{\mathbf{E}})$ is known, see [21, 23] for details on optimal test functions and proof of the norm equivalence.

To establish FE approximations of (7), we make the standard FE choice of a finite dimensional subspace $U^h(\Omega_T) \subset U(\Omega_T)$. Since $U(\Omega_T)$ consists of Hilbert spaces, we use classical FE basis functions, e.g., C^0 polynomials and/or

This error indicator has been successfully applied to a wide range of problems in both the DPG and AVS-FE methods [25, 26, 30, 31, 33].

Remark 2.1 *The size of the mixed discrete system of linear algebraic equations (18) is larger than the linear system corresponding to (17) since we do not compute optimal test functions on the fly element-by-element. An advantage of this mixed form is that its solution immediately provides an a posteriori error estimate as well as error indicators to be used in mesh adaptive strategies.*

An application of the definition of the Gateaux derivative yields the operator $B' : U(\Omega_T) \times V(\mathcal{P}_h) \rightarrow \mathbb{R}$:

$$\begin{aligned}
B'((a, \mathbf{b}, \mathbf{c}), (v, \mathbf{w}, \mathbf{p})) &\stackrel{\text{def}}{=} \sum_{K_m \in \mathcal{P}_h} \int_{K_m} \left\{ \frac{\partial a}{\partial t} v_m - \nabla v_m \cdot (\mathbf{a}\mathbf{u} + \mathbf{b}H) + \left[\frac{\partial \mathbf{b}}{\partial t} + \boldsymbol{\tau} \mathbf{b} \right] \cdot \mathbf{w}_m \right. \\
&+ \left\{ u_x \frac{\partial b_x}{\partial x} + b_x \frac{\partial u_x}{\partial x} + u_y \frac{\partial b_x}{\partial y} + b_y \frac{\partial u_x}{\partial y}, u_x \frac{\partial b_y}{\partial x} + b_x \frac{\partial u_y}{\partial x} + u_y \frac{\partial b_y}{\partial y} + b_y \frac{\partial u_y}{\partial y} \right\}^T \cdot \mathbf{w}_m \\
&- g a (\nabla \cdot \mathbf{w}_m) + \boldsymbol{\mu} \mathbf{c} : \nabla \mathbf{w}_m + \mathbf{c} : \mathbf{p}_m + \mathbf{b} \cdot (\nabla \cdot \mathbf{p}_m) \left. \right\} dx \\
&+ \oint_{\partial K_m} \left\{ (\mathbf{a}\mathbf{u} + \mathbf{b}H) \cdot \mathbf{n}_m v_m - \boldsymbol{\mu} (\mathbf{c}\mathbf{n}_m) \cdot \mathbf{w}_m \right\} ds + \oint_{\partial K_m \setminus \Gamma_{out}} g a (\mathbf{w}_m \cdot \mathbf{n}_m) ds.
\end{aligned} \tag{21}$$

Remark 2.2 *The discrete stability due to optimal test functions is unconditional in the "ideal" case in which we can exactly compute these functions. However, since this is not achievable in practical computations, we are forced to consider a practical implementation and consider an approximation of these functions [34]. Hence, the approximation of the optimal test functions leads to a potential loss of discrete stability of the approximation is not sufficiently accurate. In the DPG method, sufficient accuracy of the optimal test functions is guaranteed by the existence of (local) Fortin operators [35]. The construction of such operators is studied in great detail in [36], and its analysis was recently further refined in [37]. Generally, in DPG methods for second order PDEs, a Fortin operator's existence and thus discrete stability is ensured if the local Riesz representation problems are solved using polynomials of order $r = p + \Delta p$, where p is the degree of the trial space discretization and $\Delta p = d$ the space dimension. However, while this enrichment degree ensures the existence of the required Fortin operator, numerical evidence suggest that in most cases $\Delta p = 1$ is typically sufficient [37]. Alternative test spaces for the DPG method for singular perturbation problems are investigated in [38], even for the case of $\Delta p = 0$. Another consequence of the existence of Fortin operators is the robustness of the a posteriori error estimate through the error representation function (19) as shown in [21].*

In the AVS-FE method, numerical evidence suggests that $r = p$ is sufficient [19, 39] for convection-diffusion PDEs as well as extensive numerical experimentation for the SWE. Since the test functions are sought in a discontinuous polynomial space, using $r = p$ still results in a larger space than the trial as the discontinuous spaces contain additional degrees of freedom. Furthermore, in the limit $h \rightarrow 0$ the space $V(\mathcal{P}_h)$ is essentially L^2 , i.e., any polynomial degree above constants is inherently an enrichment of the test space.

2.3. Time Slice Approach

The numerical solution of the space-time discretizations (17) or (18) is akin to a FE discretization of a three dimensional problem. In an effort to keep the global number of degrees of freedom low, we also introduce a "time-

slice” approach as introduced for transient convection-diffusion in [40, 41] for the DPG method. Similar approaches were also employed in [15–18] for the SWE for stabilized DG and streamlined-upwind Petrov-Galerkin (SUPG) methods.

Since solution information is unidirectional in time, we are enabled to consider a partition of the temporal part of out domain Ω_T into ”slices”, see Figure 2 for an example in a spatially one dimensional domain. In each slice, starting with the one intersecting the initial time boundary Ω_0 , we solve the AVS-FE discrete problem (17) as described in Section 2.2. Each successive slice is then solved by taking the previous solutions $\zeta_{prev}^h, \mathbf{u}_{prev}^h$ as initial conditions. The slice configuration can be established in several ways, several of which are considered for the space-time DPG method in [40, 41]. Furthermore, the built-in error estimator and error indicators of the AVS-FE method lets us perform space-time mesh adaptive refinements on each individual slice. This is of particular interest in applications where the solution response varies greatly in time, thereby allowing us to adaptively refine the mesh to the required resolution in each slice. This is shown in Figure 2 with variable thickness of the slices in the t direction. In Section 4 we present

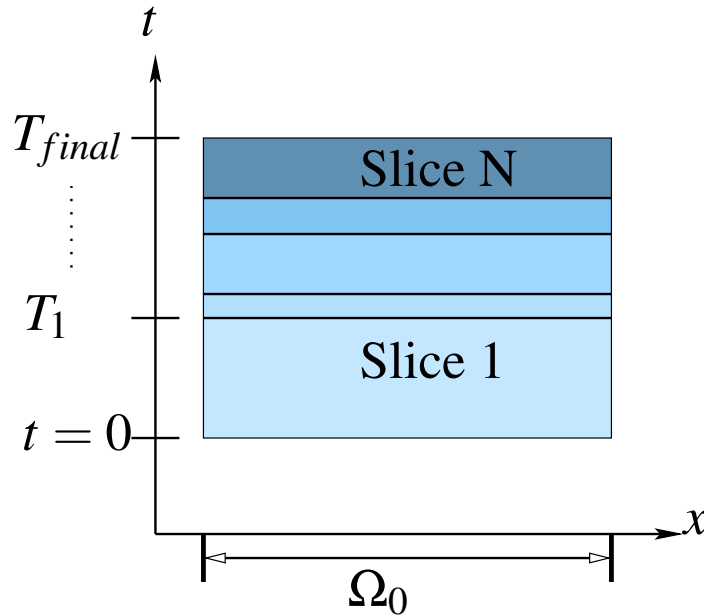


Figure 2: Partition of a space-time domain into slices.

numerical verifications for the time-slice approach.

3. A Priori Error Analysis

Here, we present *a priori* error estimates for the full space-time AVS-FE approximations for the SWE in terms of appropriate norms of the approximation error. Due to the energy norm (14) and the best approximation error of the AVS-FE method in terms of this norm, the following proofs rely on classical bounds in Hilbert spaces for continuous and discontinuous FE approximation functions. The presentation is self contained, and researchers considering a method of lines approach with AVS-FE method in space while using time stepping schemes can apply these results in their analyses. In the analysis we assume that the elevation and velocity trial variables are discretized using classical C^0

continuous FE polynomial basis functions, whereas $\boldsymbol{\sigma}^h$ is discretized using Raviart-Thomas bases. Other conforming alternatives for $\boldsymbol{\sigma}^h$ such as Brezzi-Douglas-Marini functions can also be employed with minor modifications to the following analyses and we refer to the text by Brezzi and Fortin [42] for details. We also assume that we are considering a linearized version of the SWE.

First, we introduce the best and quasi-best approximation properties of the AVS-FE method to facilitate proofs of the *a priori* bounds which are to follow.

Proposition 3.1 *Let $(\zeta, \mathbf{u}, \boldsymbol{\sigma}) \in U(\Omega_T)$ be the exact solution of the AVS-FE weak formulation (7) and $(\zeta^h, \mathbf{u}^h, \boldsymbol{\sigma}^h) \in U^h(\Omega_T)$ its corresponding AVS-FE approximation from (17) or (18). Then:*

$$\|(\zeta - \zeta^h, \mathbf{u} - \mathbf{u}^h, \boldsymbol{\sigma} - \boldsymbol{\sigma}^h)\|_{\mathbf{B}} \leq \|(\zeta - v^h, \mathbf{u} - \mathbf{w}^h, \boldsymbol{\sigma} - \mathbf{p}^h)\|_{\mathbf{B}}, \quad (22)$$

where $(v^h, \mathbf{w}^h, \mathbf{p}^h) \in U^h(\Omega_T)$.

We refer to [23] for a proof of this proposition and note that the proof relies on the definition of the energy norm (14), the Riesz problem (15), and Galerkin's orthogonality condition.

Furthermore, since the energy norm is an equivalent norm on $U(\Omega_T)$, we also have the quasi-best approximation property:

$$\|(\zeta - \zeta^h, \mathbf{u} - \mathbf{u}^h, \boldsymbol{\sigma} - \boldsymbol{\sigma}^h)\|_{U(\Omega_T)} \leq C \|(\zeta - v^h, \mathbf{u} - \mathbf{w}^h, \boldsymbol{\sigma} - \mathbf{p}^h)\|_{U(\Omega_T)}, \quad (23)$$

where the constant C is independent of the mesh and depends on norm equivalence constants between the energy norm and $\|\cdot\|_{U(\Omega_T)}$ as well as the continuity constant of a Fortin operator (see Remark 2.2).

Another key component in the following analysis is the convergence of polynomial interpolating functions. Hence, there exist a polynomial interpolation operator Π_{hp} [43]:

$$\Pi_{hp} : U \rightarrow U^{hp}. \quad (24)$$

Thus, $\Pi_h(u)$ represents an interpolant of u consisting of continuous polynomials, then [44]:

Theorem 3.1 *Let $u \in H^r(\Omega)$ and $\Pi_{hp}(u) \in U^{hp}$ be the interpolant of u (24). Then, there exists $C > 0$ such that the interpolation error can be bounded as follows:*

$$\|u - \Pi_{hp}(u)\|_{H^s(\Omega)} \leq C \frac{h^{\mu-s}}{p^{r-s}} \|u\|_{H^r(\Omega)}, \quad (25)$$

where h is the maximum element diameter, p the minimum polynomial degree of interpolants in the mesh, $s \leq r$, and $\mu = \min(p+1, r)$.

Second, we have the interpolation operator for Raviart-Thomas [42] spaces, ρ_{hp} :

$$\rho_{hp} : Q \rightarrow Q^{hp}, \quad (26)$$

Thus, $\rho_{hp}(\mathbf{q})$ represents an interpolant of \mathbf{q} consisting of polynomials which **normal** components are continuous, then [42]:

Theorem 3.2 Let $\mathbf{q} \in H(\mathbf{div}, \Omega)$ and $\rho_{hp}(\mathbf{q}) \in Q^{hp}$ be the interpolant of \mathbf{q} (26). Then, there exists $C > 0$ such that the interpolation error can be bounded as follows:

$$\exists C > 0 : \|\mathbf{q} - \rho_{hp}(\mathbf{q})\|_{H(\mathbf{div}, \Omega)} \leq Ch^n |\mathbf{q}|_{H^{n+1}(\Omega)}, \quad (27)$$

where h is the maximum element diameter and n the minimum order of Raviart-Thomas interpolants in the mesh.

The final point we highlight before proceeding with the main results of this section are on the convergence properties of interpolants of piecewise discontinuous polynomials. In [45] Rivi re *et al.* present a result analogous to Theorem 3.1 for approximations in broken Hilbert spaces.

The first *a priori* bound we present is in terms of the energy norm. While not exactly computable, it is natural to present as the energy norm is central to the stability of our method. Furthermore, we can approximate the error in the energy norm through (19). To establish error estimates in terms of the energy norm, we first establish a bound on the Riesz representers of the trial functions, i.e., the optimal test functions.

Lemma 3.1 Let $(\zeta, \mathbf{u}, \boldsymbol{\sigma}) \in U(\Omega_T)$ be the exact solution of the AVS-FE weak formulation (7) and $(\zeta^h, \mathbf{u}^h, \boldsymbol{\sigma}^h) \in U^h(\Omega_T)$ its corresponding AVS-FE approximation from (17) or (18). Then:

$$\|(\zeta - \zeta^h, \mathbf{u} - \mathbf{u}^h, \boldsymbol{\sigma} - \boldsymbol{\sigma}^h)\|_{\mathbf{B}} \leq C \frac{h^{\mu-1}}{p_{\mathbf{u}}^{r-1}}, \quad (28)$$

where h is the maximum element diameter; $\mu = \min(p_{\mathbf{u}} + 1, r)$, $p_{\mathbf{u}}$ the minimum polynomial degree of approximation of \mathbf{u}^h and ζ^h in the mesh, and r the minimum regularity of the solution components $(\hat{e}, \hat{\boldsymbol{\varepsilon}}, \hat{\mathbf{E}})$ of the distributional PDE underlying the Riesz representation problem (15).

Proof: The RHS of (22) can be bounded by the RHS of (22) can be bounded by the error in the Riesz representers of the exact and approximate AVS-FE trial functions by the energy norm equivalence in (16), and the map induced by the Riesz representation problem (15) to yield:

$$\|(\zeta - \zeta^h, \mathbf{u} - \mathbf{u}^h, \boldsymbol{\sigma} - \boldsymbol{\sigma}^h)\|_{\mathbf{B}} \leq C \|(\hat{e} - \hat{e}^h, \hat{\boldsymbol{\varepsilon}} - \hat{\boldsymbol{\varepsilon}}^h, \hat{\mathbf{E}} - \hat{\mathbf{E}}^h)\|_{V(\mathcal{P}_h)},$$

where $(\hat{e}, \hat{\boldsymbol{\varepsilon}}, \hat{\mathbf{E}}) \in V(\mathcal{P}_h)$ are the exact Riesz representers of $(\zeta, \mathbf{u}, \boldsymbol{\sigma})$ through (15), and $(\hat{e}^h, \hat{\boldsymbol{\varepsilon}}^h, \hat{\mathbf{E}}^h) \in V^*(\mathcal{P}_h)$ are the approximate Riesz representers of $(\zeta^h, \mathbf{u}^h, \boldsymbol{\sigma}^h)$ through a FE discretization of (15). Hence, the constant C depends on a Fortin type operator [36] which measures the degree of loss of stability between the continuous and discrete problems. The definition of the norm $\|\cdot\|_{V(\mathcal{P}_h)}$ in (12) and its equivalence to the norm in (13) then gives:

$$\|(\zeta - \zeta^h, \mathbf{u} - \mathbf{u}^h, \boldsymbol{\sigma} - \boldsymbol{\sigma}^h)\|_{\mathbf{B}} \leq C \{ \|\hat{e} - \hat{e}^h\|_{H^1(\mathcal{P}_h)} + \|\hat{\boldsymbol{\varepsilon}} - \hat{\boldsymbol{\varepsilon}}^h\|_{H^1(\mathcal{P}_h)} + \|\hat{\mathbf{E}} - \hat{\mathbf{E}}^h\|_{H(\mathbf{div}, \mathcal{P}_h)} \}.$$

Since $\|\cdot\|_{H(\mathbf{div}, \mathcal{P}_h)} \leq \|\cdot\|_{H^1(\mathcal{P}_h)}$, we get:

$$\|(\zeta - \zeta^h, \mathbf{u} - \mathbf{u}^h, \boldsymbol{\sigma} - \boldsymbol{\sigma}^h)\|_{\mathbf{B}} \leq C \{ \|\hat{e} - \hat{e}^h\|_{H^1(\mathcal{P}_h)} + \|\hat{\boldsymbol{\varepsilon}} - \hat{\boldsymbol{\varepsilon}}^h\|_{H^1(\mathcal{P}_h)} + \|\hat{\mathbf{E}} - \hat{\mathbf{E}}^h\|_{H^1(\mathcal{P}_h)} \}.$$

Now, we pick $(\hat{e}^h, \hat{\boldsymbol{\varepsilon}}^h, \hat{\mathbf{E}}^h)$ to be polynomial interpolants and apply the bounds in [45] for the discontinuous polynomials to get:

$$\|(\zeta - \zeta^h, \mathbf{u} - \mathbf{u}^h, \boldsymbol{\sigma} - \boldsymbol{\sigma}^h)\|_{\mathbf{B}} \leq C \left\{ \frac{h^{\mu_{\hat{e}}-1}}{p_{\hat{e}}^{r_{\hat{e}}-1}} + \frac{h^{\mu_{\hat{\boldsymbol{\varepsilon}}}-1}}{p_{\hat{\boldsymbol{\varepsilon}}}^{r_{\hat{\boldsymbol{\varepsilon}}}-1}} + \frac{h^{\mu_{\hat{\mathbf{E}}}-1}}{p_{\hat{\mathbf{E}}}^{r_{\hat{\mathbf{E}}}-1}} \right\},$$

where $\mu_i = \min(p_i + 1, r_i)$, r_i the regularity of the solution of the underlying distributional PDE and i denote the components $(\hat{e}, \hat{\boldsymbol{\varepsilon}}, \hat{\mathbf{E}})$. Finally, we complete the proof by noting that we that we pick the same degree p for all variables and that the term with the smallest r will dominate the error. Hence, we get the desired bound (28). \square

Second, we establish a bounds in terms of the Sobolev Norm $\|\cdot\|_{U(\Omega_T)}$.

Lemma 3.2 *Let $(\zeta, \mathbf{u}, \boldsymbol{\sigma}) \in U(\Omega_T)$ be the exact solution of the AVS-FE weak formulation (7) and $(\zeta^h, \mathbf{u}^h, \boldsymbol{\sigma}^h) \in U^h(\Omega_T)$ its corresponding AVS-FE approximation from (17) or (18). Then:*

$$\|(\zeta - \zeta^h, \mathbf{u} - \mathbf{u}^h, \boldsymbol{\sigma} - \boldsymbol{\sigma}^h)\|_{U(\Omega_T)} \leq C \left\{ \frac{h^{\mu-1}}{p_{\mathbf{u}}^{r-1}} + h^n \right\}, \quad (29)$$

where h is the maximum element diameter, $\mu = \min(p + 1, r)$, p the minimum polynomial degree of approximation of \mathbf{u}^h and ζ^h in the mesh, r the minimum regularity of the solution components \mathbf{u} and ζ of the underlying distributional SWE PDEs, and $n = p_{\mathbf{u}} - 1$ the minimum order of the Raviart-Thomas elements in the mesh.

Proof: By the quasi-best approximation property (23):

$$\|(\zeta - \zeta^h, \mathbf{u} - \mathbf{u}^h, \boldsymbol{\sigma} - \boldsymbol{\sigma}^h)\|_{U(\Omega_T)} \leq C \|(\zeta - v^h, \mathbf{u} - \mathbf{w}^h, \boldsymbol{\sigma} - \mathbf{p}^h)\|_{U(\Omega_T)},$$

the definition of the norm on $U(\Omega_T)$ (12) leads to :

$$\|(\zeta - \zeta^h, \mathbf{u} - \mathbf{u}^h, \boldsymbol{\sigma} - \boldsymbol{\sigma}^h)\|_{U(\Omega_T)} \leq C \{ \|\zeta - v^h\|_{H^1(\Omega_T)} + \|\mathbf{u} - \mathbf{w}^h\|_{H^1(\Omega_T)} + \|\boldsymbol{\sigma} - \mathbf{p}^h\|_{H(\text{div}, \Omega)} \},$$

by choosing functions for v^h, \mathbf{w}^h that are polynomial interpolants as in (24), and Raviart-Thomas functions for \mathbf{p}^h (26).

An application of Theorem 3.1 with $s = 1$ and Theorem 3.2 then gives:

$$\|(\zeta - \zeta^h, \mathbf{u} - \mathbf{u}^h, \boldsymbol{\sigma} - \boldsymbol{\sigma}^h)\|_{U(\Omega_T)} \leq C \left\{ \frac{h^{\mu_\zeta-1}}{p_\zeta^{r-1}} + \frac{h^{\mu_{\mathbf{u}}-1}}{p_{\mathbf{u}}^{r-1}} + h^n \right\}.$$

In the AVS-FE method, we always pick $p_{\mathbf{u}} = p_\zeta$, then considering only the largest of the fractions, the bound (29) follows and the proof is complete. \square

Last, we have error bounds in weaker norms, in this case L^2 norms, we apply the Aubin-Nitsche lift [46, 47] for the errors in $\zeta - \zeta^h$ and $\mathbf{u} - \mathbf{u}^h$. Whereas for the stress variable $\boldsymbol{\sigma} - \boldsymbol{\sigma}^h$, we rely on established bounds for Raviart-Thomas approximations found in [42]. Thus, the following can be established:

Proposition 3.2 *Let $(\zeta, \mathbf{u}, \boldsymbol{\sigma}) \in U(\Omega_T)$ be the exact solution of the AVS-FE weak formulation (7) and $(\zeta^h, \mathbf{u}^h, \boldsymbol{\sigma}^h) \in U^h(\Omega_T)$ its corresponding AVS-FE approximation from (17) or (18). Then:*

$$\|(\zeta - \zeta^h, \mathbf{u} - \mathbf{u}^h, \boldsymbol{\sigma} - \boldsymbol{\sigma}^h)\|_{L^2(\Omega_T)} \leq C \left\{ \frac{h^{\mu_\zeta-1}}{p_\zeta^{r-1}} + \frac{h^{\mu_{\mathbf{u}}}}{p_{\mathbf{u}}^{r-1}} + h^{n+1} \right\}, \quad (30)$$

where h is the maximum element diameter, $\mu_\zeta = \min(p_\zeta + 1, r_\zeta)$, p_ζ the minimum polynomial degree of approximation of ζ^h in the mesh, r_ζ the minimum regularity of the ζ of the underlying distributional SWE PDEs, , $\mu_{\mathbf{u}} = \min(p_{\mathbf{u}} +$

$1, r_{\mathbf{u}})$, $p_{\mathbf{u}}$ the minimum polynomial degree of approximation of \mathbf{u}^h in the mesh, $r_{\mathbf{u}}$ the minimum regularity of the \mathbf{u} of the underlying distributional SWE PDEs, and $n = p_{\mathbf{u}} - 1$ the minimum order of the Raviart-Thomas elements in the mesh. where h is the maximum element diameter.

□

The individual terms corresponding to the error in the velocity and $\boldsymbol{\sigma}$ are optimal in sense that it will result in convergence of the same order as their underlying polynomial interpolants. However, inspection of the term corresponding to the elevation reveals that it is sub optimal by one order. The reason is the regularity of a dual solution corresponding to this variable with an L^2 source is an order lower than the regularity of the dual solution corresponding to \mathbf{u} since the SWE contain derivatives of ζ of first order only.

Remark 3.1 *To conclude this section, we make an important remark on the AVS-FE approximations for the variable $\boldsymbol{\sigma}^h$. For convex domains Ω_T and smooth sources \mathbf{f} , the regularity of $\boldsymbol{\sigma}$ is higher than the $H(\mathbf{div}, \Omega)$ dictated by the weak form (7), i.e., $H^1(\Omega)$. Thus, it is appropriate to use C^0 continuous basis functions as advocated in [19]. As the application of the SWE often in complex coastal domains which are highly non regular, users of this method should use $H(\mathbf{div}, \Omega)$ conforming approximations such as Raviart-Thomas elements as a general rule-of-thumb in coastal domains. As in [42], the minimum order of the Raviart-Thomas elements is one order below the polynomial order for the approximate velocity. Hence, increasing the order of these elements above this does not increase the accuracy as the bounds on $\boldsymbol{\sigma} - \boldsymbol{\sigma}^h$ depend on the order of the velocity approximations.*

4. Numerical Verifications

In this section, we present numerical verifications for the AVS-FE method and the SWE. First, we consider several academic problems to ascertain convergence behavior under both uniform and adaptive mesh refinements. Finally, we consider a series of common physical benchmark problems for shallow water models from literature. While the *a priori* error estimates are established based on a linearized SWE, we consider only the full nonlinear case here as a linear SWE is generally not appropriate in physical applications of interest. For all verifications, we solve the saddle point system (18). All numerical experiments presented here are performed using the FE solver FEniCS [48]. To converge to the nonlinear SWE solutions, we employ the Portable, Extensible Toolkit for Scientific Computation (PETSc) library Scalable Nonlinear Equations Solvers (SNES) [49, 50] within FEniCS. To minimize the errors of these iterations, we set the nonlinear convergence tolerance to the value 10^{-14} . Based on our experience this typically leads to a converged solution in less than 6 nonlinear iterations.

4.1. Numerical Asymptotic Convergence Studies

To establish the convergence properties of the AVS-FE method applied to the SWE, we consider a case where the bathymetry is assumed to be constant equal to zero, i.e., $H = \zeta$. We consider a case in which the exact elevation is:

$$\zeta_{ex} = \cos(x + y - t), \quad (31)$$

whereas both components of the velocity vector \mathbf{u}_{ex} are:

$$u_{ex} = \sin(x + y + t). \quad (32)$$

The other parameters we pick are $\mu = 10^{-5}$ and $\tau_{bf} = 1$, the spatial domain is the unit square and the temporal domain is from $t = 0s$ to $t = 0.5s$. The exact solutions are then used to establish proper boundary conditions and source terms for the SWE. In the FE approximation, we employ classical Lagrange bases for ζ^h , \mathbf{u}^h , and $\boldsymbol{\sigma}^h$ since in this case the smooth solutions make C^0 regularity a valid choice for discretization of $H(\mathbf{div}, \Omega)$. Since we solve (18), we also need to specify functions spaces for the error representation function, in this case we pick discontinuous Lagrange polynomials for all components of this space of the same polynomial degree as the velocity. The initial mesh consists of six tetrahedron elements to which we perform uniform mesh refinements to ascertain the asymptotic convergence rates of applicable norms of the numerical approximation errors. In Figure 3, we present the convergence results in

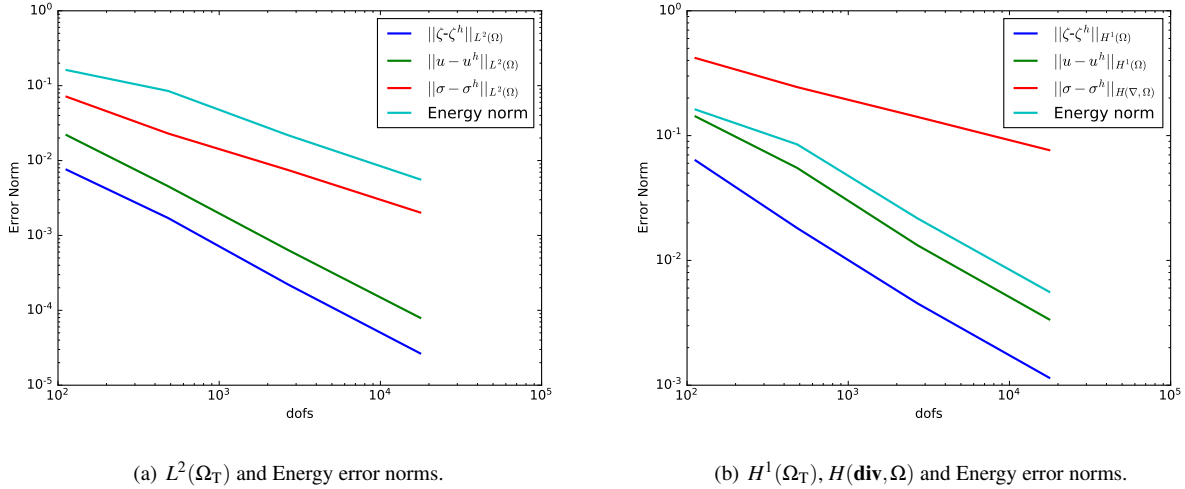


Figure 3: Error convergence results for uniform h -refinements for the SWE using polynomial approximations that are quadratic for ζ^h , \mathbf{u}^h and linear for $\boldsymbol{\sigma}^h$.

several error norms, with the observed rates of convergence listed in Table 1.

The rates of the energy norm, $\|(\zeta - \zeta^h, \mathbf{u} - \mathbf{u}^h, \boldsymbol{\sigma} - \boldsymbol{\sigma}^h)\|_{L^2(\Omega_T)}$ and $\|(\zeta - \zeta^h, \mathbf{u} - \mathbf{u}^h, \boldsymbol{\sigma} - \boldsymbol{\sigma}^h)\|_{U(\Omega)}$ are as predicted by the *a priori* estimates of Section 3. Also note that the rates of the individual error norms are of the same order as their underlying polynomial interpolants. In particular we point out that the rate observed for $\|\zeta - \zeta^h\|_{L^2(\Omega_T)}$ is an order higher than expected from an Aubin-Nitche lift (see Proposition 3.2). We also point out that the error in the energy norm converges at a higher rate than $\|\boldsymbol{\sigma} - \boldsymbol{\sigma}^h\|_{H(\mathbf{div}, \Omega)}$. Inspection of the proof of Lemma 3.1 reveals that the error in the energy norm does not the order of the Raviart-Thomas/ C^0 approximations used for $\boldsymbol{\sigma}^h$ but rather the polynomial degree of the error representation function/ optimal test function. We have also performed verification for the time slice approach of Section 2.3 in which we perform uniform mesh refinements on each slice and note that the results are essentially indistinguishable from those presented in Figure 3 for this exact solution.

Table 1: Error convergence rates corresponding to Figure 3.

Norm	Observed rate
$\ \zeta - \zeta^h\ _{L^2(\Omega_T)}$	3
$\ \mathbf{u} - \mathbf{u}^h\ _{L^2(\Omega_T)}$	3
$\ \boldsymbol{\sigma} - \boldsymbol{\sigma}^h\ _{L^2(\Omega)}$	2
$\ (\zeta - \zeta^h, \mathbf{u} - \mathbf{u}^h, \boldsymbol{\sigma} - \boldsymbol{\sigma}^h)\ _{L^2(\Omega_T)}$	2
$\ \zeta - \zeta^h\ _{H^1(\Omega_T)}$	2
$\ \mathbf{u} - \mathbf{u}^h\ _{H^1(\Omega_T)}$	2
$\ \boldsymbol{\sigma} - \boldsymbol{\sigma}^h\ _{H(\text{div}, \Omega)}$	1
$\ (\zeta - \zeta^h, \mathbf{u} - \mathbf{u}^h, \boldsymbol{\sigma} - \boldsymbol{\sigma}^h)\ _{U(\Omega_T)}$	1
$\ (\zeta - \zeta^h, \mathbf{u} - \mathbf{u}^h, \boldsymbol{\sigma} - \boldsymbol{\sigma}^h)\ _B$	2

4.2. Adaptive Mesh Refinement

In this section, we present several numerical verifications for adaptive mesh refinement. We employ the built-in error indicators of the AVS-FE method (20) and the adaptive strategy of Dörfler [51].

First, we consider a stationary problem on the domain $\Omega = (0, 0) \times (1, 1)$, and an exact solution given by:

$$\begin{aligned}
 \zeta^{ex}(x, y) &= \cos(x - xy), \\
 u_x^{ex}(x, y) &= \cos^2(\pi x + y) \sin^2(\pi x^3 + y), \\
 u_y^{ex}(x, y) &= u_x^{ex}(x, y).
 \end{aligned} \tag{33}$$

We elect to consider a stationary problem here to ensure a meaningful presentation of the resulting adapted mesh. In Figure 4 the components of this exact solution are presented. The The initial mesh consists of 2 equal triangular elements, we pick continuous quadratic polynomial bases for ζ^h , \mathbf{u}^h , first order Raviart-Thomas bases for $\boldsymbol{\sigma}^h$, and discontinuous quadratic polynomial bases for the components of the error representation function. The physical parameters in this case are $\mu = 10^{-9}$ and $\tau_{bf} = 1$. In Figure 5, the final adapted mesh, after 50 refinements, is shown along with the convergence history of the refinement process. Comparison of mesh in Figure 5(b) and the exact velocity component $u_x^{ex}(x, y)$ in Figure 4(a) shows that the refinement process leads to a mesh that is highly refined in the regions of high velocity magnitude.

To highlight the capabilities of the AVS-FE method of performing local time stepping, i.e., space-time mesh adaptivity, we consider the limiting case for the SWE of purely convective flow. Hence, we set $\mu = 0$, $\tau_{bf} = 1$, and the final time $T = 1.0s$, and we consider the exact solutions given in (32) and (31). The initial mesh consists of six space-time tetrahedrons using quadratic polynomial basis functions for ζ^h , \mathbf{u}^h , linear polynomials for $\boldsymbol{\sigma}^h$, and discontinuous quadratic polynomial bases for the error representation function. We perform a total of eight mesh refinements, and report convergence histories in Figure 6. Space-time mesh adaptive refinements using the built-in error estimate are able to appropriately refine the mesh to minimize the AVS-FE numerical approximation errors as indicated by the

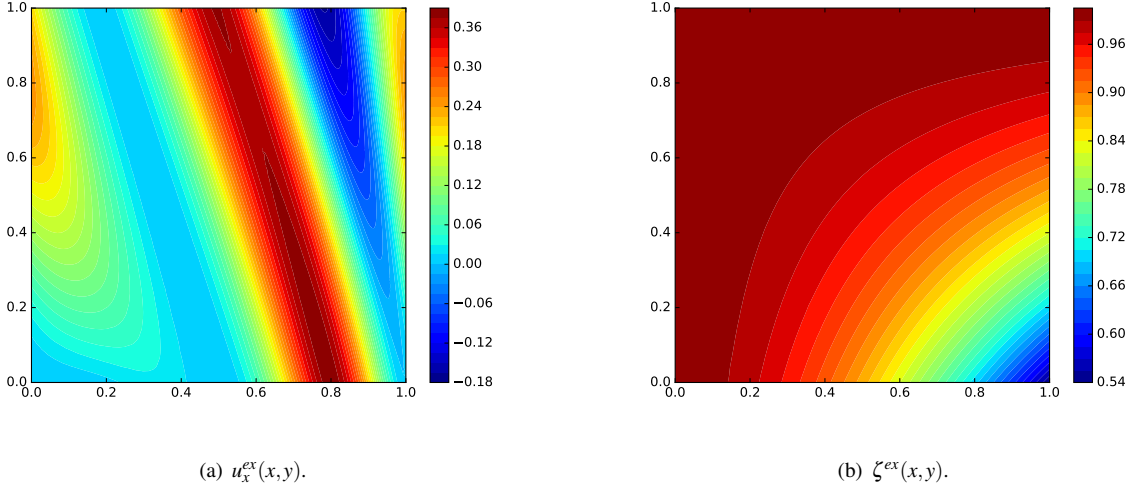


Figure 4: Exact solution components.

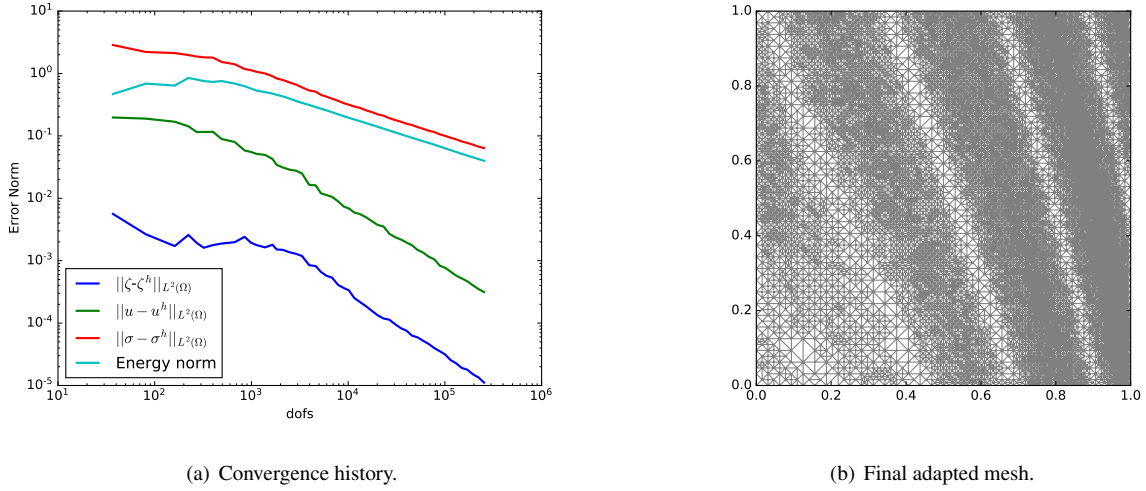
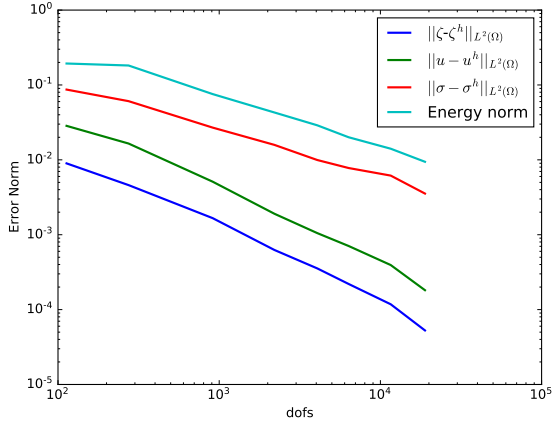


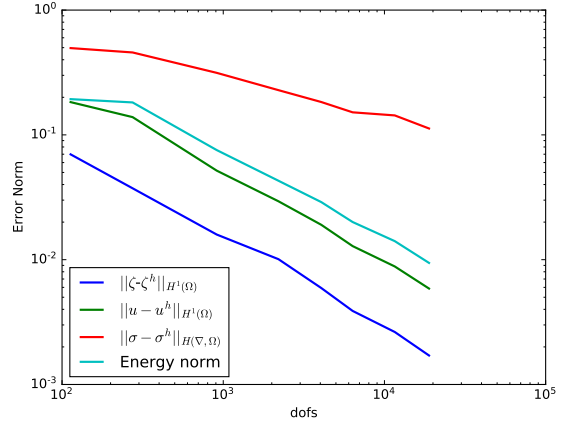
Figure 5: Results of the adaptive scheme applied to a stationary problem.

results in Figure 6.

Next, we consider a verification of the time slice approach introduced in Section 2.3, we again consider the problem as in the preceding verification, $\mu = 10^{-5}$, $\tau_{bf} = 1$, with a final time of 4s. To compare the full space-time and the space-time slices, we solve the problem using both approaches employing adaptive mesh refinements according to the built-in error indicators (20) and the same Dörfler marking strategy. For the full space-time method, the initial mesh consists of 12 tetrahedron elements and we perform a total of six mesh refinements. Conversely, for the time slice approach, we partition the space-time domain into eight equal slices discretized using 12 tetrahedron elements. In both cases, we use quadratic polynomial basis functions for ζ^h , \mathbf{u}^h , linear polynomials for σ^h , and discontinuous quadratic polynomial bases for the error representation function. Inspection of Figure 8 and 7 shows that in this case,

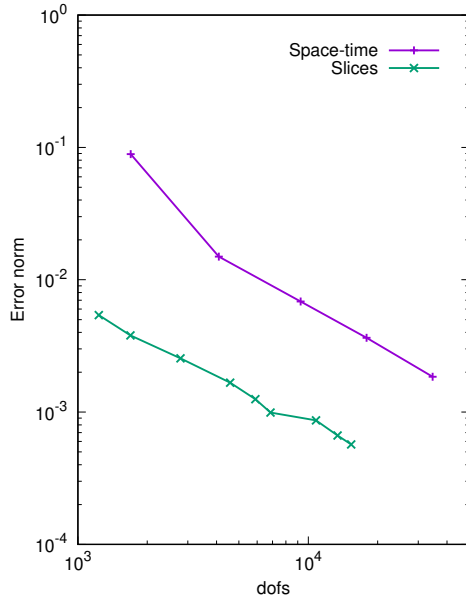


(a) $L^2(\Omega_T)$ and Energy error norms.

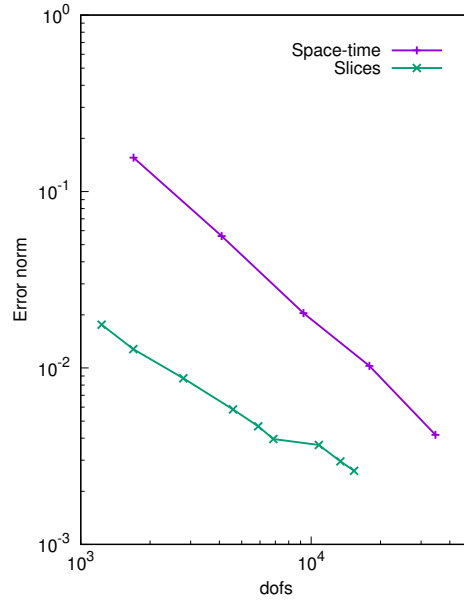


(b) $H^1(\Omega_T)$, $H(\mathbf{div}, \Omega)$ and Energy error norms.

Figure 6: Error convergence results for adaptive h -refinements for the purely convective flow regime.



(a) $\|\zeta - \zeta^h\|_{L^2(\Omega_T)}$.



(b) $\|\mathbf{u} - \mathbf{u}^h\|_{L^2(\Omega_T)}$.

Figure 7: Error convergence results comparing the space-time and time slice approaches.

the time slice approach is about an order of magnitude more accurate for the L^2 errors in ζ and \mathbf{u} . Furthermore, the number of degrees of freedom is also significantly lower for the slices than for the full space-time approach. We have observed that for problems where the final time is less than one second, the two approaches yield essentially the same accuracy. However, as this example shows, once the final time becomes larger, the time slice approach is superior.

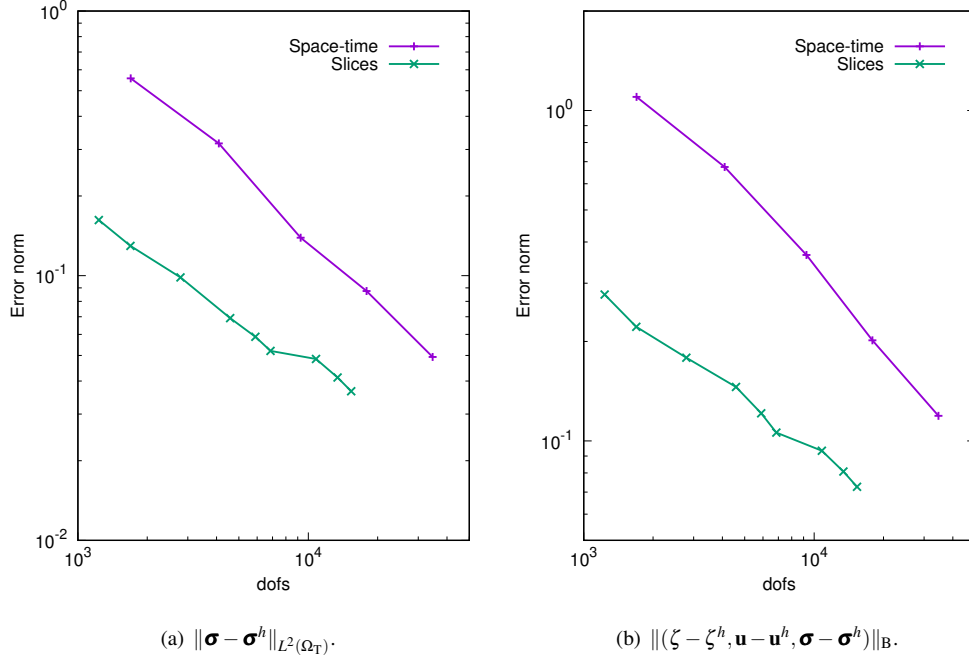


Figure 8: Error convergence results comparing the space-time and time slice approaches.

4.3. Lake At Rest

In cases of variable bathymetry $h_b(\mathbf{x})$, a common concern in the approximation of the SWE is the ability to preserve the steady state of a lake-at-rest throughout the time stepping procedures commonly employed. Numerical approximations that preserve this steady state are referred to as being well balanced [52, 53]. We consider a two-dimensional case $\Omega = (0, 1m) \times (0, 1m)$, with physical parameters $\mu = 10^{-5}m$ and $\tau_b = 1s^{-1}$, and boundary conditions:

$$\begin{aligned}
 \zeta_0 &= 0, \\
 u_0 &= 0, \\
 u &= 0, \text{ on } \partial\Omega, \\
 \zeta &= 1m, \text{ on } \partial\Omega.
 \end{aligned} \tag{34}$$

Consequently, there are no sources to induce flow in this physical example. The bathymetry is $h_b(\mathbf{x}) = 2m - h_0(\mathbf{x})$, where h_0 is:

$$h_0(\mathbf{x}) = \begin{cases} 62.5 \frac{1}{m^3} (x - 0.3m)(x - 0.7m)(y - 0.3m)(y - 0.7), & \text{if } (0.3m < x < 0.7m) \wedge (0.3m < y < 0.7m) \\ 0, & \text{otherwise} \end{cases}. \tag{35}$$

The final time is set to 10s. We consider a space-time mesh partition consisting of 150 space-time tetrahedrons such that the "width" of the elements in the time direction are equal to 10s. The resulting errors in elevation and velocity are shown in Table 2. The L^2 errors are vanishingly small, leading us to conclude that this scheme is well balanced.

Table 2: Elevation and velocity errors for the lake at rest.

$\ \zeta - \zeta^h\ _{L^2(\Omega_T)}$	$\ \mathbf{u} - \mathbf{u}^h\ _{L^2(\Omega_T)}$
$9.02 \cdot 10^{-15}$	$4.00 \cdot 10^{-13}$

4.4. Tidal Fluctuations

An important source impacting the flows governed by the SWE are tidal forces, as the hurricane storm surge can be greatly increased by tidal fluctuations. Hence, it is critical that the AVS-FE approximations of the SWE are able to accurately reproduce phenomena corresponding to tidal fluctuations. To this end, we consider a model problem from [10] to facilitate comparison with existing FE methods for the SWE. The spatial domain is a one-dimensional channel $\Omega = (x_L, x_R) = (0, 10000m)$ with a constant bathymetry $h_b(\mathbf{x}) = 10m$, the physical parameters are $\mu = 25m$ and $\tau_b = 0.01s^{-1}$, and the initial and boundary conditions are:

$$\begin{aligned}
 \zeta_0 &= 0, \\
 u_0 &= 0, \\
 \boldsymbol{\sigma}(0, t) &= 0, \\
 u(10000m, t) &= 0, \\
 \zeta(0, t) &= 0.1\cos(t\alpha)m,
 \end{aligned} \tag{36}$$

where $\alpha = 0.00014051891708$. Since this is a one-dimensional problem, the spaces $H(\mathbf{div}, \Omega)$ and $H^1(\Omega)$ coincide and we use C^0 polynomial approximations for all trial variables. As the period of tidal fluctuations are on the order of days, we consider a case in which the fluctuations occur over 7 days, i.e., the space-time domain is $\Omega_T = (0, 10000m) \times (0, 604800s)$. In the corresponding AVS-FE discretization of the space-time domain we employ a uniform mesh of $2(25 \times 400)$ triangular elements, which corresponds to a "time step" of 1512 seconds. In Figure 9, the water column elevation at $x = 800m$ is shown for the full 7 day time span. As expected, the resulting tidal fluctuation leads to a sinusoidal elevation profile and at $x = 800m$, the wave amplitude is slightly damped from the incoming tidal wave. Correspondingly, in Figure 10, the corresponding velocity is presented. Here we observe that the highest velocity magnitudes occur slightly before and after the peak tidal elevation. Visual inspection of the results in [10], where a coupled discontinuous and continuous Galerkin method is considered, compared with Figures 9 and 10 shows comparable behavior. However, the time step used in [10] is $0.25s$ in Euler's method, i.e., the total number of time steps over seven days is roughly 2.4 million, whereas the AVS-FE solution is obtained in a single solution step.

4.5. Dam Break

As a final numerical verification, we consider another commonly applied benchmark problem found in literature [54], known as a dam break problem. We consider a one-dimensional case, in which a $2000m$ channel is divided by a dam separating two distinct water levels, i.e., $\Omega = (x_L, x_R) = (0, 2000m)$. In Figure 11 the set up for the problem

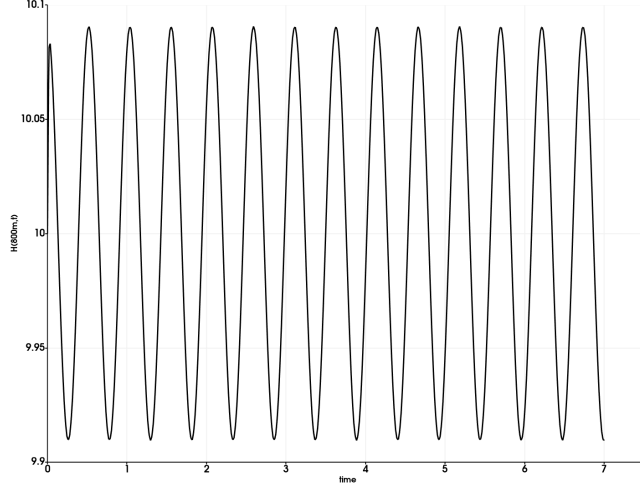


Figure 9: $H^h(800m, t)$ (m).

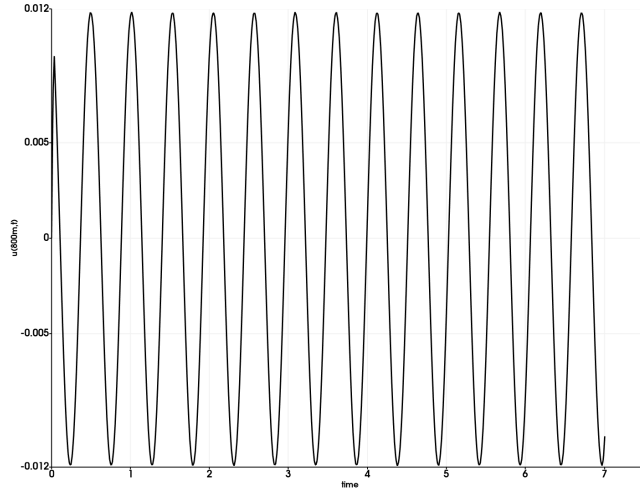


Figure 10: $u^h(800m, t)$ ($\frac{m}{s}$).

is shown. At $t = 0s$, the dam is removed to simulate its total failure allowing the water to flow unconstrained into the lower reservoir. The physical parameters are $v = 10^{-2}m$ and $\tau_b = 1s^{-1}$, we consider a constant bathymetry $h_b(\mathbf{x}) = 0$, and the initial and boundary conditions are:

$$\begin{aligned}
 \zeta_0 &= 10m, & x &\leq 1000m \\
 \zeta_0 &= 5m, & x &> 1000m \\
 u_0 &= 0, \\
 u(0, t) &= 0, \\
 \zeta(2000m, t) &= 0.
 \end{aligned} \tag{37}$$

Hence, we expect sharp interfaces in the resulting velocity and elevation fields, i.e., shocks to develop. We consider

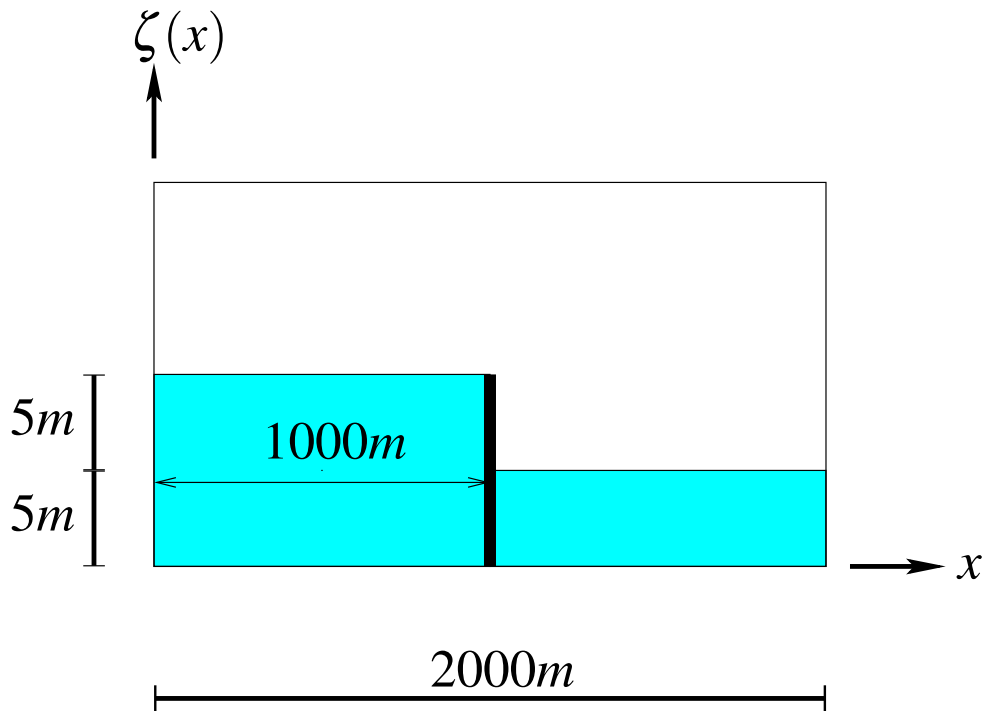


Figure 11: Dam break problem spatial domain.

the final time to be $T = 200s$, i.e., the space-time domain is $\Omega_T = (0, 2000m) \times (0, 200s)$. The corresponding AVS-FE discretization employs a uniform mesh of $2(800 \times 35)$ triangular elements and quadratic polynomial approximations for all variables, except the stress which is linear. In Figure 12, we present the elevation profile for select times. As

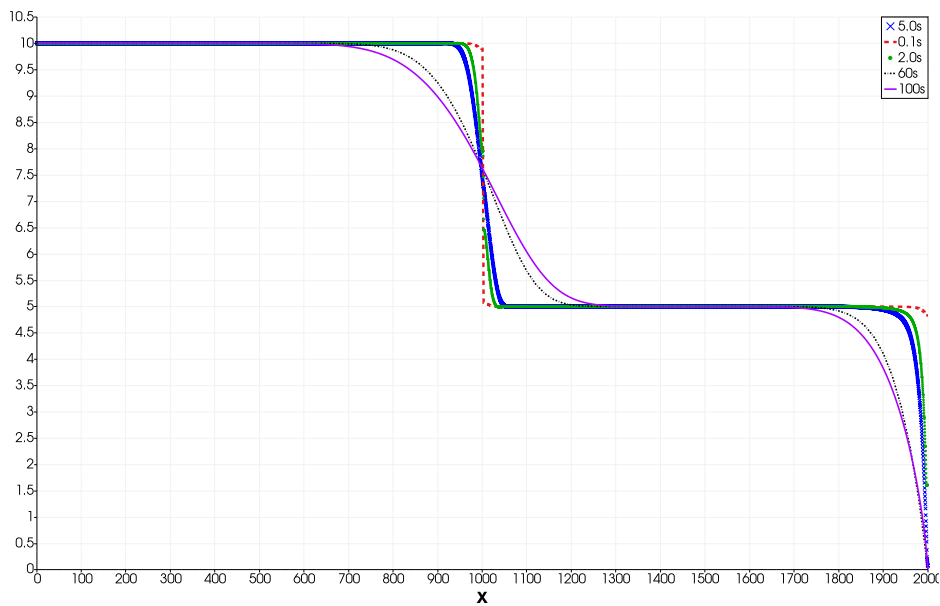


Figure 12: $\zeta^h(x,t)$ at various times.

time progresses, the elevation profile stretches out as expected from the boundary and initial conditions. Shortly after

the simulated dam break, at $t = 0.1$ seconds, the elevation profile does not exhibit any noticeable oscillations leading to an accurate representation of the shock. Comparison with the results in [54], which uses slightly different boundary and initial conditions, shows good agreement based on visual inspection.

5. Conclusions

We have introduced an unconditionally stable space-time FE method for the SWE, the AVS-FE method. This Petrov-Galerkin method derives its stability from the DPG concept of optimal test functions. The flexibility of the DPG method allows us to establish continuous and stable FE approximations in both space and time by breaking the test space and introducing a Riesz representation problem governing the optimal test functions. Compared to existing FE technologies for the SWE we do not need to consider surrogate models such as the diffusive wave model or perform arduous problem-dependent analysis to establish proper stabilization parameters to achieve discrete stability.

Consideration of a linearized SWE allows us to establish well posedness of the AVS-FE weak formulation in terms of the energy norm induced by the sesquilinear form by employing the DPG philosophy. Furthermore, for the linearized problem, we establish *a priori* error estimates. The convergence behavior predicted by these estimates is confirmed through a sequence of numerical convergence studies for the full nonlinear SWE. In the case of asymptotic h -convergence, we observe optimal rates for all applicable norms of the numerical approximation errors. The built-in error estimate and corresponding error indicators of the AVS-FE approximation error in terms of the energy norm allows us to pursue space-time adaptive mesh refinement strategies.

In an effort to keep the computational cost of the space-time AVS-FE approximations low, we also consider a technique in which we partition the space-time domain into space-time slices. While the space-time AVS-FE method allows us to perform local time stepping in the form of adaptive mesh refinements in space-time, the time slice approach allows further localization of the space-time mesh refinements, which now occur on each individual slice. We present numerical verifications in which we consider and compare the space-time and space-time slice approaches to each other. These verifications show that the time slice approach becomes preferable for longer simulations. Note that what constitutes a long simulation is problem dependent. For the SWE and the verifications we consider here our experience indicates that the threshold is around one second.

We have considered space-time adaptive mesh refinements using a built-in error estimate of the AVS-FE. However, we are not limited to this type of error estimator, and any *a posteriori* error estimation technique can be applied. In particular, we envision the use of Goal-Oriented error estimates, and their error indicators, of local quantities of interest. These types of estimates have been established in [39] for the AVS-FE method and linear stationary convection-diffusion problems. For the transient portion of the domain, goal-oriented adaptive algorithms such as those developed by Muñoz-Matute *et. al* [55] show great potential.

The results presented in this paper serves as a proof-of-concept of the space-time AVS-FE method applied to the SWE. In particular, we have presented numerical verifications of two important physical processes governed by the SWE, tidal fluctuations and that of a dam failure. In addition to these physical examples, we have also verified the well balanced property of the AVS-FE method applied to the SWE numerically in Section 4.3. Hence, we aim to establish a

establish a new paradigm of the application of DPG methods in the mathematical modeling of storm surge events. As these physical processes are complex, occur in complex coastal domains, and exhibit significant temporal variability (e.g., due to changes in wind or rainfall), the local time stepping allowed in the space-time methods is likely to be an important factor to be exploited in future works. Coupling mechanisms such as those established by Choudhary in [56] and by Dawson and Proft in [10] are likely to lead to efficient algorithms in the modeling of storm surge by coupling, e.g., the AVS-FE method and HDG methods [18, 57].

Acknowledgements

This work has been supported by the United States National Science Foundation - NSF PREEVENTS Track 2 Program, under NSF Grant Number 1855047.

References

- [1] J. Peraire, O. Zienkiewicz, K. Morgan, Shallow water problems: a general explicit formulation, *International Journal for Numerical Methods in Engineering* 22 (3) (1986) 547–574.
- [2] M. Kawahara, H. Hirano, K. Tsubota, K. Inagaki, Selective lumping finite element method for shallow water flow, *International Journal for Numerical Methods in Fluids* 2 (1) (1982) 89–112.
- [3] D. R. Lynch, W. G. Gray, A wave equation model for finite element tidal computations, *Computers & fluids* 7 (3) (1979) 207–228.
- [4] R. A. Luettich, J. J. Westerink, N. W. Scheffner, et al., Adcirc: an advanced three-dimensional circulation model for shelves, coasts, and estuaries. report 1, theory and methodology of ADCIRC-2DD1 and ADCIRC-3DL (1992).
- [5] A. Samii, K. Kazhyken, C. Michoski, C. Dawson, A comparison of the explicit and implicit hybridizable discontinuous Galerkin methods for nonlinear shallow water equations, *Journal of Scientific Computing* 80 (3) (2019) 1936–1956.
- [6] G. J. Gassner, A. R. Winters, D. A. Kopriva, A well balanced and entropy conservative discontinuous Galerkin spectral element method for the shallow water equations, *Applied Mathematics and Computation* 272 (2016) 291–308.
- [7] N. Wintermeyer, A. R. Winters, G. J. Gassner, D. A. Kopriva, An entropy stable nodal discontinuous Galerkin method for the two dimensional shallow water equations on unstructured curvilinear meshes with discontinuous bathymetry, *Journal of Computational Physics* 340 (2017) 200–242.
- [8] E. J. Kubatko, S. Bunya, C. Dawson, J. J. Westerink, Dynamic p-adaptive Runge–Kutta discontinuous Galerkin methods for the shallow water equations, *Computer Methods in Applied Mechanics and Engineering* 198 (21-26) (2009) 1766–1774.

- [9] X. Wu, J. Chan, E. Kubatko, High-order entropy stable discontinuous Galerkin methods for the shallow water equations: curved triangular meshes and gpu acceleration, arXiv preprint arXiv:2005.02516 (2020).
- [10] C. Dawson, J. Proft, Discontinuous and coupled continuous/discontinuous Galerkin methods for the shallow water equations, *Computer Methods in Applied Mechanics and Engineering* 191 (41-42) (2002) 4721–4746.
- [11] C. Dawson, J. Proft, Discontinuous/continuous Galerkin methods for coupling the primitive and wave continuity equations of shallow water, *Computer methods in applied mechanics and engineering* 192 (47-48) (2003) 5123–5145.
- [12] P. B. Bochev, M. D. Gunzburger, *Least-Squares Finite Element Methods*, Vol. 166, Springer Science & Business Media, 2009.
- [13] G. Starke, A first-order system least squares finite element method for the shallow water equations, *SIAM journal on numerical analysis* 42 (6) (2005) 2387–2407.
- [14] S.-J. Liang, T.-W. Hsu, Least-squares finite-element method for shallow-water equations with source terms, *Acta Mechanica Sinica* 25 (5) (2009) 597–610.
- [15] F. Ribeiro, R. Castro, A. Galeão, A. Loula, L. Landau, A space-time finite element formulation for shallow water equations with shock-capturing operator, in: *IV World Congress, Argentina, 1998*.
- [16] F. Ribeiro, A. Galeão, R. Castro, L. Landau, Finite elements for shallow water equations: stabilized formulations and computational aspects, *WIT Transactions on Engineering Sciences* 29 (1970).
- [17] S. Takase, K. Kashiya, S. Tanaka, T. E. Tezduyar, Space–time SUPG formulation of the shallow-water equations, *International Journal for Numerical Methods in Fluids* 64 (10-12) (2010) 1379–1394.
- [18] H. Arabshahi, Space-time hybridized discontinuous Galerkin methods for shallow water equations, Ph.D. thesis (2016).
- [19] V. M. Calo, A. Romkes, E. Valseth, Automatic variationally stable analysis for FE computations: an introduction, in: Barrenechea G., Mackenzie J. (eds) *Boundary and Interior Layers, Computational and Asymptotic Methods BAIL 2018*, Springer, 2020, pp. 19–43.
- [20] L. Demkowicz, J. Gopalakrishnan, A class of discontinuous Petrov-Galerkin methods. Part I: The transport equation, *Computer Methods in Applied Mechanics and Engineering* 199 (23) (2010) 1558–1572.
- [21] C. Carstensen, L. Demkowicz, J. Gopalakrishnan, A posteriori error control for DPG methods, *SIAM Journal on Numerical Analysis* 52 (3) (2014) 1335–1353.
- [22] L. Demkowicz, J. Gopalakrishnan, Analysis of the DPG method for the Poisson equation, *SIAM Journal on Numerical Analysis* 49 (5) (2011) 1788–1809.

- [23] L. Demkowicz, J. Gopalakrishnan, A class of discontinuous Petrov–Galerkin methods. II. Optimal test functions, *Numerical Methods for Partial Differential Equations* 27 (1) (2011) 70–105.
- [24] L. Demkowicz, J. Gopalakrishnan, A class of discontinuous Petrov–Galerkin methods. Part III: Adaptivity, *Applied numerical mathematics* 62 (4) (2012) 396–427.
- [25] E. Valseth, C. Dawson, An unconditionally stable space–time FE method for the Korteweg–de Vries equation, *Computer Methods in Applied Mechanics and Engineering* 371 (2020) 113297.
- [26] C. Carstensen, P. Bringmann, F. Hellwig, P. Wriggers, Nonlinear discontinuous Petrov–Galerkin methods, *Numerische Mathematik* 139 (3) (2018) 529–561.
- [27] R. Falconer, An introduction to nearly horizontal flows, *Coastal, estuarial and harbour engineers’ reference book* (1993) 27–36.
- [28] N. Praagman, Numerical solution of the shallow water equations by a finite element method, Ph.D. thesis, Technische Hogeschool Delft (1979).
- [29] I. Babuška, Error-bounds for finite element method, *Numerische Mathematik* 16 (1971) 322–333.
- [30] C. Carstensen, L. Demkowicz, J. Gopalakrishnan, Breaking spaces and forms for the DPG method and applications including Maxwell equations, *Computers & Mathematics with Applications* 72 (3) (2016) 494–522.
- [31] N. V. Roberts, L. Demkowicz, R. Moser, A discontinuous Petrov–Galerkin methodology for adaptive solutions to the incompressible Navier–Stokes equations, *Journal of Computational Physics* 301 (2015) 456–483.
- [32] L. F. Demkowicz, J. Gopalakrishnan, An overview of the discontinuous Petrov Galerkin method, in: *Recent developments in discontinuous Galerkin finite element methods for partial differential equations*, Springer, 2014, pp. 149–180.
- [33] E. Valseth, A. Romkes, A. R. Kaul, A stable FE method for the space-time solution of the Cahn–Hilliard equation, Preprint Submitted to *Journal of Computational Physics*, arXiv preprint arXiv:2006.02283 (2020).
- [34] J. Gopalakrishnan, W. Qiu, An analysis of the practical DPG method, *Mathematics of Computation* 83 (286) (2014) 537–552.
- [35] D. Boffi, F. Brezzi, M. Fortin, et al., *Mixed finite element methods and applications*, Vol. 44, Springer, 2013.
- [36] S. Nagaraj, S. Petrides, L. F. Demkowicz, Construction of DPG Fortin operators for second order problems, *Computers & Mathematics with Applications* 74 (8) (2017) 1964–1980.
- [37] L. Demkowicz, P. Zanotti, Construction of DPG Fortin operators revisited, *Computers & Mathematics with Applications* (2020).

- [38] J. Salazar, J. Mora, L. Demkowicz, Alternative enriched test spaces in the DPG method for singular perturbation problems, *Computational Methods in Applied Mathematics* 19 (3) (2019) 603–630.
- [39] E. Valseth, A. Romkes, Goal-oriented error estimation for the automatic variationally stable FE method for convection-dominated diffusion problems, Accepted in *Computers and Mathematics with Applications*, arXiv preprint arXiv:2003.10904 (2020).
- [40] T. E. Ellis, Space-time discontinuous Petrov-Galerkin finite elements for transient fluid mechanics, Ph.D. thesis (2016).
- [41] T. E. Ellis, L. Demkowicz, J. Chan, R. D. Moser, Space-time DPG: Designing a method for massively parallel CFD, ICES report, The Institute for Computational Engineering and Sciences, The University of Texas at Austin (2014) 14–32.
- [42] F. Brezzi, M. Fortin, *Mixed and Hybrid Finite Element Methods*, Vol. 15, Springer-Verlag, 1991.
- [43] I. Babuška, M. Suri, The hp version of the finite element method with quasiuniform meshes, *ESAIM: Mathematical Modelling and Numerical Analysis-Modélisation Mathématique et Analyse Numérique* 21 (2) (1987) 199–238.
- [44] J. T. Oden, J. N. Reddy, *An introduction to the mathematical theory of finite elements*, Dover Publications, 2012.
- [45] B. Rivière, M. F. Wheeler, V. Girault, Improved energy estimates for interior penalty, constrained and discontinuous Galerkin methods for elliptic problems. part i, *Computational Geosciences* 3 (3-4) (1999) 337–360.
- [46] J.-P. Aubin, *Analyse fonctionnelle appliquée. tome i* (1987).
- [47] J. Nitsche, On Dirichlet problems using subspaces with nearly zero boundary conditions, in: *The mathematical foundations of the finite element method with applications to partial differential equations*, Elsevier, 1972, pp. 603–627.
- [48] M. S. Alnæs, J. Blechta, J. Hake, A. Johansson, B. Kehlet, A. Logg, C. Richardson, J. Ring, M. E. Rognes, G. N. Wells, The FEnics project version 1.5, *Archive of Numerical Software* 3 (100) (2015) 9–23.
- [49] S. Abhyankar, J. Brown, E. M. Constantinescu, D. Ghosh, B. F. Smith, H. Zhang, *Petsc/ts: A modern scalable ode/dae solver library*, arXiv preprint arXiv:1806.01437 (2018).
- [50] S. Balay, S. Abhyankar, M. F. Adams, J. Brown, P. Brune, K. Buschelman, L. Dalcin, A. Dener, V. Eijkhout, W. D. Gropp, D. Karpeyev, D. Kaushik, M. G. Knepley, D. A. May, L. C. McInnes, R. T. Mills, T. Munson, K. Rupp, P. Sanan, B. F. Smith, S. Zampini, H. Zhang, H. Zhang, *PETSc users manual*, Tech. Rep. ANL-95/11 - Revision 3.12, Argonne National Laboratory (2019).
URL <https://www.mcs.anl.gov/petsc>

- [51] W. Dörfler, A convergent adaptive algorithm for Poisson's equation, *SIAM Journal on Numerical Analysis* 33 (3) (1996) 1106–1124.
- [52] V. Michel-Dansac, C. Berthon, S. Clain, F. Foucher, A well-balanced scheme for the shallow-water equations with topography or manning friction, *Journal of Computational Physics* 335 (2017) 115–154.
- [53] R. J. LeVeque, Balancing source terms and flux gradients in high-resolution godunov methods: the quasi-steady wave-propagation algorithm, *Journal of computational physics* 146 (1) (1998) 346–365.
- [54] C. T. Jacobs, M. D. Piggott, Firedrake-fluids v0. 1: numerical modelling of shallow water flows using an automated solution framework, *Geoscientific Model Development* 8 (3) (2015) 533–547.
- [55] J. Muñoz-Matute, V. M. Calo, D. Pardo, E. Alberdi, K. G. van der Zee, Explicit-in-time goal-oriented adaptivity, *Computer Methods in Applied Mechanics and Engineering* 347 (2019) 176–200.
- [56] G. K. Choudhary, et al., Coupled atmospheric, hydrodynamic, and hydrologic models for simulation of complex phenomena, Ph.D. thesis (2019).
- [57] G. S. Jones, J. J. Lee, S. Rhebergen, A space-time hybridizable discontinuous Galerkin method for linear free-surface waves, *arXiv preprint arXiv:1910.07315* (2019).